Applied Surface Science 599 (2022) 154052

Contents lists available at ScienceDirect

Applied Surface Science

journal homepage: www.elsevier.com/locate/apsusc

Full Length Article

Unraveling the effects of Fe and Mn promoters on the tungstated zirconia catalyst: A DFT study

Karina G. Madrigal-Carrillo [a], Juan I. Rodríguez [a,*], Martha L. Hernández-Pichardo [b], Elisa Jimenez-Izal [c,d,*]

[a] Escuela Superior de Física y Matemáticas, Instituto Politécnico Nacional, Edificio 9, U.P. A.L.M, Col. San Pedro Zacatenco, Ciudad de México, C.P. 07738, México
[b] Instituto Politécnico Nacional, ESIQIE, Av. IPN S/N Zacatenco, México City, 07738, México
[c] Polimero eta Material Aurreratuak: Fisika, Kimika eta Teknologia Saila, Kimika Fakultatea, Euskal Herriko Unibertsitatea (UPV/EHU) and Donostia International Physics Center (DIPC), M. de Lardizabal Pasealekua 3, Donostia, Euskadi, Spain
[d] IKERBASQUE, Basque Foundation for Science, Bilbao, Euskadi, Spain

ARTICLE INFO

Keywords:
DFT
Tungstated zirconia
Catalysis
Alkane isomerization
WOx clusters
Deprotonation

ABSTRACT

Periodic DFT calculations are performed to unravel the effect of the incorporation of Fe and Mn into the tungstated zirconia catalyst, $(WO_3)_x/ZrO_2$ (x = 1,3), in their electronic, geometric, and catalytic properties. Our results suggest that both Mn and Fe have a proclivity to occupy the same positions and thus both metals will compete for the same adsorption sites. The addition of Fe or Mn slightly destabilizes the WO_3 monomer while stabilizes the $(WO_3)_3$ trimer. Hence, medium size clusters, which are the most catalytically active species, will be more sinter resistant in the presence of the promoters, leading to catalysts with longer lifetimes. The computed deprotonation energies evidence that the overall Brønstead acidity is increased upon the addition of the dopant atoms. It is proposed that the metals lead to a reduction of WZ and induce a local spin density imbalance.The function as redox initiators of these metals is confirmed.

1. Introduction

Solid acid catalysts are widely used in the chemical and petrochemical industry due to the ability of these materials to catalyze a variety of reactions such as alkylation, isomerization, cracking, hydrotreating, and dehydration of alcohols [1-3]. An important class of such catalysts consists of transition metal oxides with platinum inclusions to prevent their deactivation [4]. Among these solids, anion-modified metal oxides such as sulfated zirconia (SZ) and tungstated zirconia (WZ) are highly active and selective.

Sulfated and tungstated zirconia catalysts can operate at low temperatures compared to acidic zeolites and achieve greater selectivity to the desired products. However, the main drawback of SZ is the tendency to degrade due to the loss of sulfur, in addition to its poor stability and regeneration. Such features limit its applicability in isomerization and alkylation processes. In this vein, WZ is a convenient alternative because it is more selective and, although it requires a higher operating temperature, it does not decompose at temperatures below 850 °C [5,6]. Moreover, in the case of isomerization reactions, tungstated zirconia has proven to be an efficient choice to replace liquid acids in the production of bi-ramified isoalkanes due to its high activity and selectivity.

Regarding the nature of the active sites in this catalytic system, it has been generally accepted that the WO_x clusters developed on the zirconia surface are responsible for the formation of acidic sites [7]. Moreover, the increase in catalytic activity has been associated with a slight reduction in the tungsten phase, which results in a protonation variation, since stronger Brønsted acid sites are generated when tungsten oxide is reduced [8]. Therefore, the ability of surface oxide domains to accept or redistribute electron density is critical to their function as acid catalysts. This charge redistribution capacity is intimately related to the domain size of the WO_x nanostructures [5,9]. Recently, a novel alkoxide-free sol–gel method to synthesize mesoporous Pt/WO_3-ZrO_2 catalysts, with a better control over the size of the WO_x clusters, confirmed that polytungstates with an intermediate domain size provided the best activity in terms of the conversion and selectivity in the n-hexane hydroisomerization [10]. DFT calculations of model catalysts showed that the origin of such a size effect arises from a combination of two factors [10]. On the one hand, the reducibility and the Brønsted acid strength increases as the size of the WO_x species increases. On the other hand, the most acidic sites are those located at the interface between the two

* Corresponding authors.
E-mail addresses: jirodriguezh@ipn.mx (J.I. Rodríguez), elisa.jimenez@ehu.es (E. Jimenez-Izal).

https://doi.org/10.1016/j.apsusc.2022.154052
Received 7 April 2022; Received in revised form 17 June 2022; Accepted 21 June 2022
Available online 23 June 2022

oxides. Therefore, intermediate WO_x cluster sizes offer a favorable tradeoff between the Brønsted acid strength and the number of such active sites.

The catalytic performance of sulfated and tungstated zirconia catalysts can be boosted by incorporating diverse promoters, such as gallium, aluminum, iron or manganese [11-23]. SZ doped with Fe and Mn, for example, catalyzes isomerization reactions two to three orders of magnitude faster than undoped SZ [15,16,20,22]. Regarding WZ, several works have shown that the incorporation of Fe and Mn improves the paraffin isomerization activity of these catalysts [13,14,17-19,21,23,24]. Nevertheless, as in the SZ case, the nature of the promoting effect of these metals remains highly debated.

Hernández-Pichardo et al. carried out several experimental studies on the WZ promoted with Fe and Mn [17,18,21,24]. Their works suggested that Fe^{3+} and Mn^{3+} cations modify the interaction of the WO_x species with the support. They argue that the incorporation of these promoters into the WZ catalysts modifies the anchoring of the tungstated species on the zirconia surface, which allows the stability of the tetragonal zirconia and prevents the growth of WO_x crystals. The catalytic behavior, however, is not a linear function of the composition of Mn or Fe, and a low promoter content is required to achieve better activity and selectivity [17,18]. Indeed, at higher metal loadings, the corresponding oxides are formed, which are catalytically inactive, producing a yield decrease.

In addition, other experimental studies have suggested that Fe and Mn-containing WZ catalysts play a role as a redox initiator, affecting the dehydrogenation activity of the materials [13]. The stabilization of tetragonal zirconia was also pinpointed as a key factor influencing the catalytic performance of WZ [14,25]. Finally, the acidity, reducibility and dispersion of the WO_x layer was also observed to change by the dopants [23].

It is noticeable that, depending on the synthesis method, the addition of these metals to tungstated zirconia leads to different effects. However, there are important discrepancies in the literature regarding the influence of Fe and Mn on the structural and catalytic properties of the WZ. How Fe and Mn modify the WO_x/ZrO_2 catalyst is not clear yet and there is a need to achieve a better understanding of the structure–activity relationship of the promoted WZ, to hopefully lead to the design of more active and selective catalysts.

The objective of this work is to achieve an atomistic description of the effect of Fe and Mn on the WO_x/ZrO_2 acid catalyst. Through state-of-the-art density functional theory (DFT) calculations, which include the Hubbard U (DFT + U) and Grimme dispersion (D3) corrections, the electronic and structural properties of the promoted catalyst are studied. The new insight provides a basis for predictive models of future acid-supported metal oxide catalytic materials that will lead to the design of more active and selective catalysts.

2. Computational Methods

All calculations are performed with PW-DFT using the PBE exchange-correlation functional [26], as formulated in the generalized gradient approximation (GGA), and the PAW pseudopotentials [27,28], implemented in the VASP package [29-32]. To correctly describe the dispersion interactions, the Grimme's DFT-D3 scheme is used [33]. The Hubbard correction is well known for improving the description of highly correlated systems with respect to pure functional and bringing them closer to hybrid functionals in terms of precision. We use the effective Hubbard parameter U = 4 eV for the d electrons Zr atoms, as implemented in Duvarev's simplified scheme [34], which ensures a good qualitative description of the structure and electronic properties of Zr oxides [35,36]. All the calculations are spin polarized. The most stable facet of tetragonal ZrO_2 (101) is modeled using a previously optimized ZrO_2 supercell, corresponding to a $Zr_{450}O_{300}$ composition [37]. For the geometry optimization, the top two layers of the slab and the clusters $(WO_3)_X$ on top of it are allowed to relax, while the bottom layers of the support are fixed at the positions of the bulk. A 12 Å vacuum separation is added between cells repeated in the z-direction to avoid interactions between the replicas of the slab pattern. For geometry relaxation (SCF) procedure, the convergence criteria is set up to 10^{-5} (10^{-6}) eV, the cutoff energy of the plane wave was 450 eV and a 1x1x1 Γ-centered k points grid is used in the calculations, given the large dimension of the unit cells. Atomic charges are calculated using Bader's partition method [38]. In order to unravel the effect of the incorporation of Fe and Mn into the $(WO_3)_x/ZrO_2$ catalyst (x=1,3), first of all the model is set up, as explained in the Supporting Information.

Different adsorption energies of the modeled systems (E_{ads}) are calculated according to the following equations:

$$E_{ads}(M) = E(M+((WO_3)_x/ZrO_2) \quad - E((WO_3)_x/ZrO_2) - E(M)_{gas} \tag{1}$$

$$E_{ads}((WO_3)_x) = E(M+((WO_3)_x/ZrO_2) \quad - E(M/ZrO_2) - E((WO_3)_x)_{gas} \tag{2}$$

$$E_{ads}(M-(WO_3)_x) = E(M+((WO_3)_x/ZrO_2) \quad - E(ZrO_2) - E(M-(WO_3)_x)_{gas} \tag{3}$$

where $E(M+((WO_3)_x/ZrO_2)$ is the energy of the catalyst with the metal deposited, $E((WO_3)_x/ZrO_2)$ is the energy of the cluster supported on the surface, $E(M\text{-}ZrO_2)$ is the energy of the bare metal atom deposited on the ZrO_2 support, $E(M)_{gas}$ is the energy of Fe or Mn in gas phase, $E((WO_3)_x)_{gas}$ the energy of the tungsten oxide cluster in gas phase and $E(M\text{-}(WO_3)_x)_{gas}$ the energy of the $M\text{-}(WO_3)_x$ complex in gas phase.

Finally, the deprotonation energies are calculated as:

$$DPE = E_{SystemH} - E_{System^-} \tag{4}$$

where $E_{SystemH}$ is the energy of $M\text{-}(WO_3)_x/ZrO_2$ (M = Fe, Mn; x = 1,3) with a H bonded in its neutral form, and E_{System^-} is the energy of the corresponding conjugate base, i. e., $M\text{-}(WO_3)_x/ZrO_2$ in its anionic form.

3. Results and discussion

In order to determine the preferred binding site for Fe and Mn on the tungstated zirconia catalyst, one Fe(Mn) atom is added to the most stable WO_3/ZrO_2 and $(WO_3)_3/ZrO_2$ structures (which were previously determined in ref. 10). The incorporation of Fe or Mn is performed by including a single metal atom in every symmetrically non-equivalent site corresponding to a 1:1 and 1:3 metal:W ratio. Upon the inclusion of Fe into the monomer, two competitive binding sites are found, depicted in Fig. 1. In the putative global minimum Fe is located at the subsurface site below the WO_3 monomer, binding with neighboring O atoms and slightly displacing them. In the second isomer, which is only 0.02 eV less stable than the global minimum, Fe is on top of the ZrO_2 surface, in between the two oxides. In this case, the metal bonds with two O atoms and the W atom of the cluster, as well as to one O and one Zr from the surface. The Fe-O bond lengths in the global minimum are in the range of 2.06 and 2.37 Å, while for the second isomer bond lengths are in the range of 1.94 and 2.00 Å. Note that in both configurations, the monomer is in a bridging position with two of the monomer's O atoms bonding to the closest surface Zr atoms, while W bonds to a surface O atom (see Fig. 1). Similar features are found in other local minima, shown in the Supporting Information (Figure S3). Regarding the tungsten trioxide trimer, the most stable binding site for Fe is found to be on top of the $(WO_3)_3$ cluster, where iron is surrounded by oxygen atoms in a quasi-planar geometry (see Fig. 1). The resulting Fe-O bond lengths are between 1.85 and 1.98 Å. Overall, the inclusion of Fe on the supported mono- and tri-tungsten oxide catalysts has minimal effect on their geometry.

Adsorbed Mn on the WZ catalyst tends to be surrounded by oxygen atoms, as in the case of Fe. The most stable $Mn\text{-}(WO_3)_x/ZrO_2$ (x = 1,3) are shown in Fig. 1 and other local minima are shown in Figure S3. In the monomer, the preferred binding site for manganese is at the interface between the two oxides, similar to the second most stable $Fe\text{-}WO_3/ZrO_2$

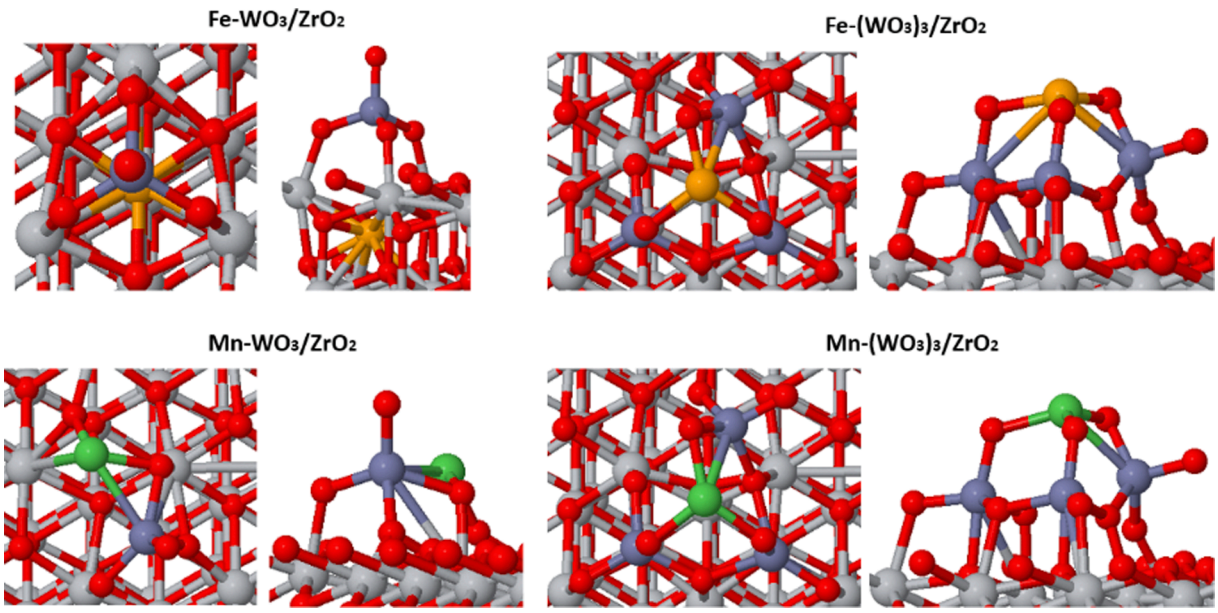

Fig. 1. Side and top view of the most stable Fe and Mn doped $(WO_3)_x/ZrO_2$ catalyst (x = 1,3). W, O, Zr, Fe and Mn atoms are shown in blue, red, gray, orange, and green, respectively.

structure. Mn bonds to oxygen atoms with bond lengths of 1.93 and 1.98 Å, and to one W atom with a bond distance of 2.65 Å. The structure with the metal at the zirconia subsurface site, analogous to the Fe-WO_3/ZrO_2 global minimum, is thermodynamically considerably less stable (>1.2 eV when comparing structures on cells containing two support layers).

When the size of the $(WO_3)_x$ cluster is increased up to the trimer, manganese binds on top of $(WO_3)_3$, the same preferred location as iron. Such adsorption site allows for maximizing the number of Mn-O bonds (bond lengths of 1.91–1.99 Å), in addition to one Mn-W bond (bond length of 2.65 Å). Our results suggest that both Mn and Fe have a proclivity to occupy the same binding positions. Experimentally, it is found that the best strategy to boost the catalytic activity and selectivity of WO_x/ZrO_2 is through the addition of either Fe or Mn, instead of adding both metals together. The reason for such behavior can be explained by considering that both metals will compete for the same adsorption sites.

We would like to highlight that only in the Fe-WO_3/ZrO_2 system, the dopant shows a preference to be incorporated into the zirconia lattice, rather than at the interface between the two oxides or on top of the tungsten oxide clusters. In previous experimental works, the lattice parameters of the tetragonal zirconia were found to increase scarcely upon the addition of Mn or Fe [21], suggesting that at least a portion of the promoters would be integrated interstitially into the zirconia lattice. We must emphasize that our DFT calculations give information on the thermodynamic stability of different species, location or conformers, and these isomers are predicted to be present in an experimental sample with different relative abundance. However, the calculations do not account for the kinetics effects or consider a larger metal coverage. Furthermore, the observed behavior in the experiments might be influenced by factors related to the synthesis method, such as the dopant incorporation procedure (i. e. impregnation or co-precipation), the dopant content, the presence of surfactants, among others.

With the aim of clarifying the effect of the promoters on the possible (de)stabilization of the tungsten oxide catalysts, several adsorption energies are computed, according to the equations (1) to (3), which are shown in Table 1. First, the adsorption of the metals on the $(WO_3)_x/ZrO_2$ catalyst, E_{ads}(M), evidence that Fe binds more strongly to the mixed oxide than Mn, and that both metals bind more strongly to the WO_3 trimer than the monomer. Hence, the promoters will have a larger tendency to bind to medium size clusters rather than to the small ones.

If the clusters were complexed with the metals before being deposited on ZrO_2, E_{ads}(M-$(WO_3)_x$) suggest that Mn-WO_x complexes would bind more strongly to the support, primarily the manganese doped trimer. For this calculation, the most stable isolated gas-phase $(M{-}WO_3)_x$ complex structures (M = Fe, Mn; x = 1,3) are determined. As can be seen in Figure S4, the preferred geometries are unchanged when going from isolated systems to the corresponding deposited species on ZrO_2. The only exception is Fe-WO_3/ZrO_2, since on the support Fe prefers to be located at the subsurface site, although the most stable gas-phase geometry is very close in energy.

Finally, the $E_{ads}((WO_3)_x)$ allows a comparison between the adsorption of these clusters to the bare support on the one hand, and a support that is pre-doped with Fe or Mn on the other hand. In this vein, if the clusters were to be adsorbed on a doped zirconia surface, different effects would be found depending on the cluster size. The mono-tungsten oxide catalysts would have a slightly weaker interaction with the doped support. Indeed, the $E_{ads}((WO_3)_x$ on the unpromoted ZrO_2 is −5.96 eV and the value is reduced to −5.46 (-5.78) eV for the Fe(Mn) doped ZrO_2. Nonetheless, the effect of the dopants is the opposite in the tri-tungsten oxide catalysts: $E_{ads}((WO_3)_x$ increases from −5.22 to 7.00 (-6.92) eV in

Table 1
Electronic and energetic properties of the most stable M-$(WO_3)_x/ZrO_2$ structures (M = Fe, Mn; x = 1,3): Bader charges on the tungsten trioxide clusters, ΔQ $(WO_3)_x$, and the metal atom (Fe or Mn), ΔQ (M) (electrons), number of unpaired electrons, Ue^-, and different adsorption energies (eV) explained in the Methods section. * data taken from Ref. [10].

	E_{ads}(M)	E_{ads}(M-$(WO_3)_x$)	$E_{ads}((WO_3)_x)$	ΔQ $(WO_3)_x$	ΔQ (M)	Ue^-
WO_3/ZrO_2	–	–	−5.96*	−0.33*	–	0
Fe-WO_3/ZrO_2	−1.99	−4.46	−5.46	−0.40	+2.55	2
Mn-WO_3/ZrO_2	−1.61	−4.62	−5.78	−0.91	+1.99	5
$(WO_3)_3$/ZrO_2	–	–	−5.22	−0.46*	–	0
Fe-$(WO_3)_3$/ZrO_2	−4.28	−5.44	−7.00	−1.46	+2.27	4
Mn-$(WO_3)_3$/ZrO_2	−3.50	−5.64	−6.92	−1.60	+2.28	3

the presence of Fe(Mn). Moreover, there is a change of tendency, since on the pristine support, the WO_3 monomers are more strongly anchored than the trimers but, upon the incorporation of the metals, the latter will be more resistant to sintering and, therefore, more stable. In fact, all the computed E_{ads} agree in predicting that the larger tungsten oxide catalysts interact more strongly with the metals and the surface, conferring them a higher stability. Therefore, both iron and manganese award a large stabilizing effect to medium size WO_x clusters, which are the most catalytically active species. Moreover, according to these results, the best strategy to anchor the clusters and reduce their tendency to sintering would be to complex them with the metallic promoters prior to their adsorption on tetragonal zirconia.

The Bader charges, summarized in Table 1 and depicted in Fig. 2, are additionally computed in order to study the influence of the promoters on the electronic properties of the acid catalyst. In the unpromoted catalyst the tungsten oxide clusters are reduced due to the charge transfer from the underlying support. The acquired charge in the trimer is larger than that in the monomer (-0.46 vs −0.33 |e|) [10]. Upon the inclusion of the metals, WO_x are further reduced. The least noticeable change occurs in Fe-WO_3/ZrO_2 because iron is located inside the support, and it is donating electrons mostly to ZrO_2. In Mn-WO_3/ZrO_2, manganese is located at the interface between tungsten oxide and zirconium oxide, and it is oxidized as a result of its interaction with both oxides. Nevertheless, in the case of M-$(WO_3)_3/ZrO_2$, since the metals are bonding only to $(WO_3)_3$, the charge acquired by the trimer is increased dramatically, reaching −1.46 and 1.60 |e| for iron and manganese doped $(WO_3)_3/ZrO_2$ respectively. Note that, as a result of the charge transfer, the charges on the oxygen atoms at W-O-Zr and at M−O−Zr interfaces are similar. The dopants slightly reduce the W atoms too. In addition, the number of unpaired electrons on the different structures evidence the presence of spin polarized states, unlike in the undoped WZ compounds, that have a closed-shell electronic structure [10]. The spin density of the most stable geometries is shown in Fig. 3. In agreement with the bader charges, the electrostatic exchange is weak in the monomers. Indeed, in M-WO_3/ZrO_2 (especially for the Fe case) most of the spin density is located on the dopant atom. When the size of the tungsten oxide cluster increases, however, spin density shows up on several oxygen atoms of the trimers. Note that the spin density imbalance is most marked in the Fe-WO_3/ZrO_2 and Mn-$(WO_3)_3/ZrO_2$ catalysts. Overall these metals reduce the WO_x catalysts and create spin polarized states on them, primarily on the medium size clusters, suggesting that they must influence the redox properties of the studied catalysts.

Finally, to gain an insight into the effect of Fe and Mn on the catalytic force of the supported mono- and tri-tungsten oxide catalysts, hydrogen is adsorbed in all the possible Brønsted acid sites (oxygen atoms) and the deprotonation energies (DPE) are computed. The deprotonation energy, i. e., the energy required to remove a proton from the solid acid to form the conjugate base and a separated proton, provides an idealized but direct measure of the Brønsted acidity. The most stable acidic sites with adsorbed hydrogen are shown in Fig. 4.

We must emphasize that charged defects in periodic calculations, such as those created after a deprotonation process, can introduce artificial interactions between defects in neighboring cells. VASP utilizes a neutralizing background charge, although it requires large supercells and several works showed that the resulting energies might be incorrect [39,40]. In addition, dipole and quadrupole corrections currently implemented in VASP have several constraints, such as their limited use to cubic supercells. Other additional artifacts arise from arbitrary energy references used for charged systems in periodic calculations [41]. For these reasons, the absolute DPE might not be fully reliable and therefore, in this work we focus and discuss the relative DPE values. Specifically, the DPE values are calculated with respect to the averaged DPE on the unpromoted monomer, whose ⟨DPE⟩ is 4.72 eV [10]. Positive values with respect to that reference are indicative of a larger DPE and thus a weakening of the acid strength, while negative Δ(DPE) indicate a smaller DPE value and thus, stronger acidity. In this way, the negative value of Δ(DPE) is directly proportional to the catalytic power of each system. All the relative deprotonation energies are plotted in Fig. 5(a) and given in Table S2.

Experimentally, it was reported that adding small amounts of metal promoters (Fe or Mn) increases alkene isomerization yield with respect to pure WZ [18,21]. Such catalytic boosting depends strongly on the metal concentration; the isomerization conversion is increased as the metal concentration increases, until reaching a maximum, and then the conversion decreases for higher metal concentrations. The maximum catalytic activity determined experimentally occurs at a 15% wt. of WO_3 and 0.5% wt. of Fe or Mn respectively (see Fig. 5(a)), which corresponds

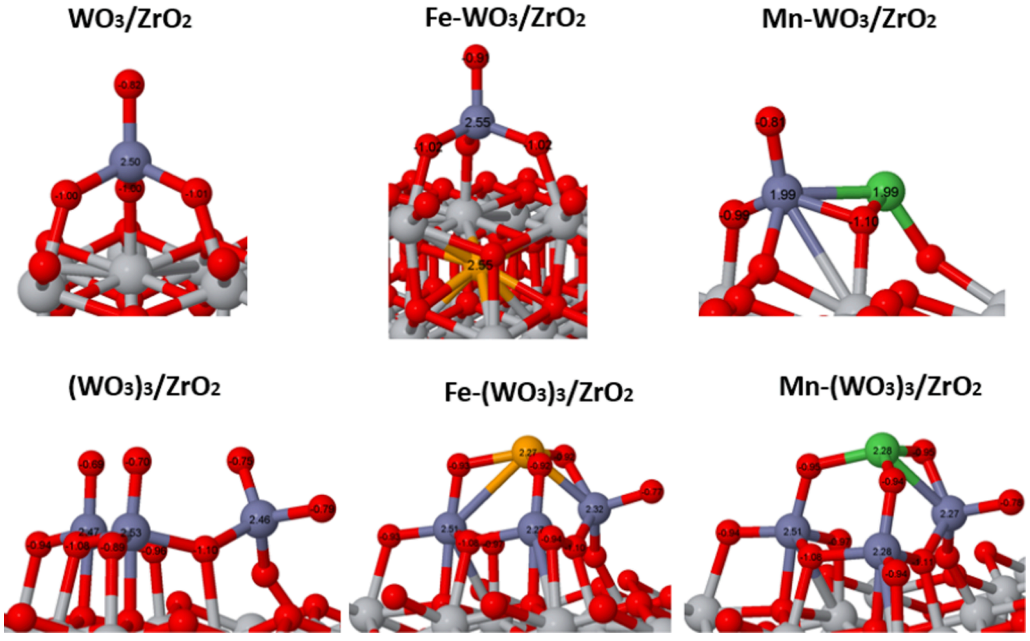

Fig. 2. Bader charges on the most stable undoped and Fe and Mn promoted $(WO_3)_x/ZrO_2$ catalyst (x = 1,3). W, O, Zr, Fe and Mn atoms are shown in blue, red, gray, orange, and green, respectively.

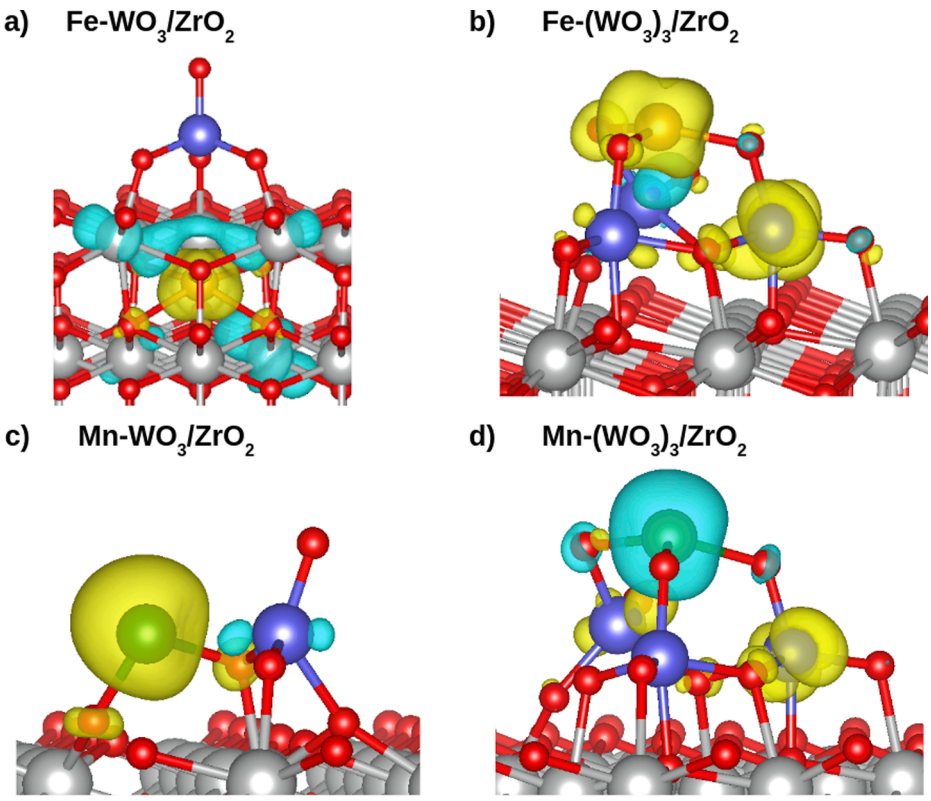

Fig. 3. Spin density on the most stable Fe and Mn doped $(WO_3)_x/ZrO_2$ catalyst (x = 1,3). Isosurface value 0.05 e/Å^3. W, O, Zr, Fe and Mn atoms are shown in blue, red, gray, orange, and green respectively.

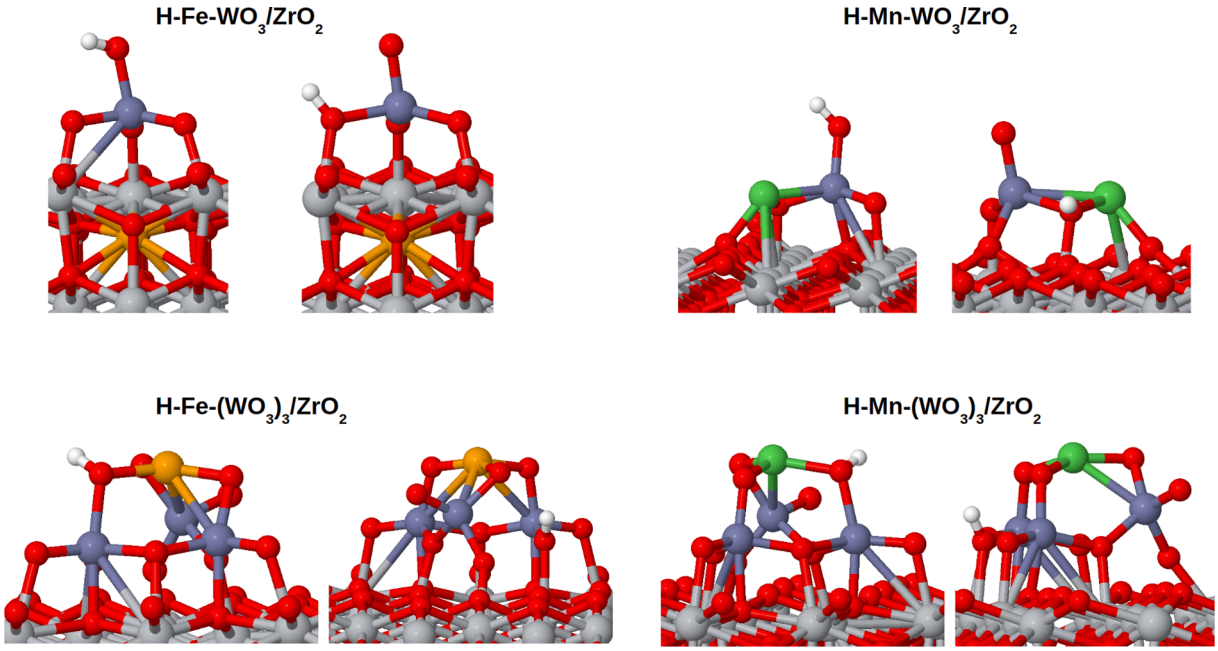

Fig. 4. Most stable top and lateral H adsorption sites on M-$(WO_3)_x/ZrO_2$ catalyst (M = Fe, Mn; x = 1,3). H, W, O, Zr, Fe and Mn atoms are shown in white, blue, red, gray, orange, and green respectively.

to an Fe(Mn)/W atomic ratio ~ 0.14. In the present models, the incorporation of Fe or Mn corresponds to a 1:1 and 1:3 metal:W ratio. Overall, our computed DPE values confirm the experimental observations as can be clearly seen in Fig. 5(b). The acid strength is systematically increased in every promoted catalyst with respect to pure WZ, which is represented by all points below zero in Fig. 5(b). Furthermore, the computed averaged deprotonation energies, ⟨DPE⟩, clearly depend on the metal concentration in agreement with the experimental data (notice that, in Fig. 5(a), the catalysts on the x-axis are ordered in terms of metal concentration). Although our theoretical study only covers one part of the metal concentration interval that is considered in the experiment, the variation of the curves in Fig. 5(b) might predict the existence of the

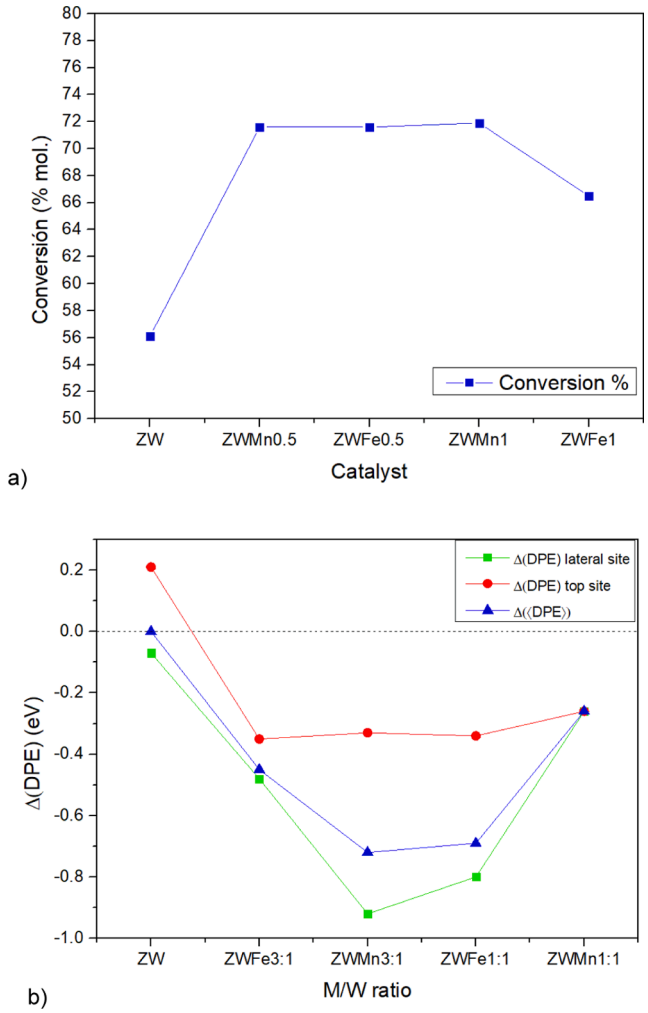

Fig. 5. (a) Experimental catalytic activity as conversion, for catalysts supported on WZ promoted with 0.0, 0.5, and 1.0 %wt. of Fe and Mn, in the n-hexane isomerization reaction at 260 °C (ref. 21). (b) computed DPEs values with respect to the DPE of unpromoted WZ (WO_3/ZrO_2 as computed in Ref. 10).

experimental maximum or "saturation point". Beyond this concentration, the metals will likely form their respective oxides and segregate from the catalyst, as was experimentally evidenced [18,21].

Finally, as it can be seen in Fig. 5(b), the computed Δ(DPE) values at the top sites are similar regardless of the specific dopant and its concentration (red curve in Fig. 5(b)), while the acidity of the lateral oxygens shows a larger variation (green curve in Fig. 5(b)). These sites are the most acidic ones in every M-$(WO_3)_x/ZrO_2$ (M = Fe, Mn; x = 1,3) catalyst, i. e., the oxygens at the interface between WO_x and ZrO_2 (see Fig. 4). Hence, the bridging W-OH-Zr groups are responsible for the strongest Brønsted acidity, as found in the unpromoted catalysts [10]. Furthermore, the largest decrease in the DPE values is found in the Fe-WO_3/ZrO_2 and Mn-$(WO_3)_3/ZrO_2$ cases. In these systems the local spin density imbalance is more marked. As shown in Fig. 3, the color change on the isosurface indicates a sign change in the spin density, so that in the blue (yellow) areas there is an accumulation of alpha (beta) electrons. Such a feature is most marked in the Fe-WO_3/ZrO_2 and Mn-$(WO_3)_3/ZrO_2$ catalysts, which exhibit the greatest variations in the acidity, regardless of the cluster size and/or metal concentration. These results taken together suggest that iron and manganese increase the acidity of the WZ catalysts, by reducing the WZ catalyst and by inducing a local spin density imbalance. Indeed, the larger reducibility of this class of catalysts has been related previously to the increase in their acidity and catalytic activity.

4. Conclusions

The catalysts used for the isomerization of alkanes are mainly solid acids such as tungstated zirconia (WO_x/ZrO_2), which has stability and activity advantages over other solid catalysts. The role of metal promoters (Fe, Mn) on these catalysts has been connected to several factors such as the formation and stabilization of carbenium ion intermediates on the surface, a higher dehydrogenation capacity, a process redox trigger, or the synergism between redox and acid sites. Many of these assumptions point to an interaction between redox sites and acid sites but, to the best of our knowledge, no clear evidence has been presented in this regard. The present work achieves an atomistic description of the effect of Fe and Mn on the WO_x/ZrO_2 acid catalyst, via state-of-the-art density functional theory calculations (DFT).

By exploring $(WO_3)_x$-ZrO_2 (x = 1,3) models, the role of the dopants on the electronic structure, tendency to sintering and acid properties of WZ is unraveled. Some effects induced by the dopant atoms might exist that cannot be explored within our models, such as the stabilization of the metastable tetragonal zirconia or the tendency to form inactive iron or manganese oxides at high metal concentrations. However, mono- and tri-tungsten oxide surface-supported cluster moldes capture a wide-range of structural and electronic features, and yet they are computationally tractable.

Our results suggest that both Mn and Fe have a proclivity to occupy the same positions. Experimentally it was found that the best strategy to boost the activities and selectivities of WO_x/ZrO_2 is through the addition of either Fe or Mn, instead of adding both metals together. The reason for such behavior can be explained by considering that both metals will compete for the same adsorption sites. In addition, the incorporation of Fe or Mn slightly destabilizes the WO_3 monomers while stabilizing the $(WO_3)_3$ trimer. Therefore, medium size clusters, which are the most catalytically active species, will be more sinter resistant in the presence of the promoters, leading to catalysts with longer lifetimes.

The computed deprotonation energies show that the overall acidity is increased upon the incorporation of the Fe and Mn dopant atoms. The found effect can be correlated with the large charge transfer of the dopant to the WZ catalyst and with an induced local spin density imbalance, associated with stronger Brønsted acidity.

Our DFT results give a quantitative basis to some of the assumptions used to explain the experimental findings on the catalytic activity boosting by adding the metal dopants. This knowledge provides the tools for the future design of more efficient catalytic materials for alkane isomerization.

Declaration of Competing Interest

The authors declare that they have no known competing financial interests or personal relationships that could have appeared to influence the work reported in this paper.

Acknowledgements

This work is supported by grant PID2020-114754GA-I00 funded by MCIN/ AEI/10.13039/501100011033 and funding provided by Gobierno Vasco-Eusko Jaurlaritza (IT1254-19). We also thank DIPC and SGI-IZO-SGIker (UPV/EHU) for the generous allocation of computational resources. The authors thankfully acknowledge also the computer resources at MareNostrum and the technical support provided by Barcelona Supercomputing Center (QHS-2021-3-0004). The authors acknowledge the Instituto Politécnico Nacional for the financial support received through project SIP-20221590. J.I.R. thanks SIP-IPN for financial support (projects SIP20210100 and SIP20221613). K.G.M.C. thanks CONACYT-Mexico for the doctorate fellowship (CVU: 745592).

Appendix A. Supplementary material

Supplementary data to this article can be found online at https://doi.org/10.1016/j.apsusc.2022.154052.

References

[1] H. Hattori, Solid acid catalysts: Roles in chemical industries and new concepts, Top. Catal. 53 (7-10) (2010) 432–438, https://doi.org/10.1007/s11244-010-9469-9.

[2] H.H. Kozo Tanabe, Makoto Misono, Yoshio Ono, Solid Acids and Bases, Elsevier, 1970. https://doi.org/10.1016/B978-0-12-683250-1.X5001-9.

[3] M.R. Guisnet, Model reactions for characterizing the acidity of solid catalysts, Acc. Chem. Res. 23 (11) (1990) 392–398, https://doi.org/10.1021/ar00179a008.

[4] J.M.P. V.M. Benitez, C.R. Vera, J.M. Grau, J.C. Yori, C.L. Pieck, Conversión de benceno de corrientes parafínicas en reactores de isomerización conteniendo catalizadores Pt/WO3-ZrO2, (2004) 10. http://www.e-petroquimica.com/trabajos/conversion_de_benceno.pdf.

[5] D.G. Barton, M. Shtein, R.D. Wilson, S.L. Soled, E. Iglesia, Structure and Electronic Properties of Solid Acids Based on Tungsten Oxide Nanostructures, J. Phys. Chem. B. 103 (4) (1999) 630–640, https://doi.org/10.1021/jp983555d.

[6] J.M.H. Enríquez, L.A.G. Serrano, R.G. Alamilla, L.A.C. Lajas, Síntesis, caracterización y evaluación catalítica de un ZrO 2 con fase monoclínica, 22 (2009) 1–9.

[7] D.G. Barton, S.L. Soled, G.D. Meitzner, G.A. Fuentes, E. Iglesia, Structural and Catalytic Characterization of Solid Acids Based on Zirconia Modified by Tungsten Oxide, J. Catal. 181 (1) (1999) 57–72, https://doi.org/10.1006/jcat.1998.2269.

[8] A. Martinez, G. Prieto, M. Arribas, P. Concepcion, J. Sanchezroyo, Influence of the preparative route on the properties of WOx–ZrO2 catalysts: A detailed structural, spectroscopic, and catalytic study, J. Catal. 248 (2) (2007) 288–302, https://doi.org/10.1016/j.jcat.2007.03.022.

[9] C.D. Baertsch, K.T. Komala, Y.-H. Chua, E. Iglesia, Genesis of Brønsted Acid Sites during Dehydration of 2-Butanol on Tungsten Oxide Catalysts, J. Catal. 205 (1) (2002) 44–57, https://doi.org/10.1006/jcat.2001.3426.

[10] J. Vera-Iturriaga, K.G. Madrigal-Carrillo, M.L. Hernández-Pichardo, J.I. Rodríguez, E. Jiménez-Izal, J.A. Montoya de la Fuente, A size-selective method for increasing the performance of Pt supported on tungstated zirconia catalysts for alkane isomerization: a combined experimental and theoretical DFT study, New J. Chem. 45 (23) (2021) 10510–10523, https://doi.org/10.1039/D1NJ01725J.

[11] X.R. Chen, C.L. Chen, N.P. Xu, C.Y. Mou, Al- and Ga-promoted WO3/ZrO2 strong solid acid catalysts and their catalytic activities in n-butane isomerization, Catal. Today. 93–95 (2004) 129–134, https://doi.org/10.1016/j.cattod.2004.06.030.

[12] J.G. Santiesteban, D.C. Calabro, C.D. Chang, J.C. Vartuli, T.J. Fiebig, R.D. Bastian, The Role of Platinum in Hexane Isomerization over Pt/FeOy/WOx/ZrO2, J. Catal. 202 (1) (2001) 25–33, https://doi.org/10.1006/jcat.2001.3229.

[13] X. Carrier, P. Lukinskas, S. Kuba, L. Stievano, F.E. Wagner, M. Che, H. Knözinger, The state of the iron promoter in tungstated zirconia catalysts, ChemPhysChem. 5 (8) (2004) 1191–1199, https://doi.org/10.1002/cphc.200400046.

[14] L.I. Kuznetsova, A.V. Kazbanova, P.N. Kuznetsov, Effect of promoters on the structure and catalytic properties of tungstated zirconia in n-heptane isomerization, Pet. Chem. 53 (5) (2013) 322–325, https://doi.org/10.1134/S0965544113050058.

[15] C.Y. Hsu, C.R. Heimbuch, C.T. Armes, B.C. Gates, A highly active solid superacid catalyst for n-butane isomerization: A sulfated oxide containing iron, manganese and zirconium, J. Chem. Soc. Chem. Commun. 02 (1992) 1645–1646, https://doi.org/10.1039/C39920001645.

[16] S.G. Ryu, B.C. Gates, N-hexane conversion catalyzed by sulfated zirconia and by iron-and manganese-promoted sulfated zirconia: Catalytic activities and reaction network, Ind. Eng. Chem. Res. 37 (1998) 1786–1792, https://doi.org/10.1021/ie970554j.

[17] M.L. Hernández-Pichardo, J.A. Montoya, P. del Angel, A. Vargas, J. Navarrete, A comparative study of the WOx dispersion on Mn-promoted tungstated zirconia catalysts prepared by conventional and high-throughput experimentation, Appl. Catal. A Gen. 345 (2) (2008) 233–240, https://doi.org/10.1016/j.apcata.2008.05.005.

[18] M.L. Hernandez-Pichardo, J.A. Montoya De La Fuente, P. Del Angel, A. Vargas, J. Navarrete, I. Hernandez, L. Lartundo, M. González-Brambila, High-throughput study of the iron promotional effect over Pt/WO x-ZrO 2 catalysts on the skeletal isomerization of n-hexane, Appl. Catal. A Gen. 431–432 (2012) 69–78, https://doi.org/10.1016/j.apcata.2012.04.023.

[19] P. Lukinskas, S. Kuba, B. Spliethoff, R.K. Grasselli, B. Tesche, H. Knözinger, Role of promoters on tungstated zirconia catalysts, Top. Catal. 23 (2003) 163–173, https://doi.org/10.1023/A:1024840808217.

[20] J.M.M. Millet, M. Signoretto, P. Bonville, Characterization of Fe-promoted sulfated zirconia catalysts used for the n-butane isomerization by XPS and Mössbauer spectroscopies, Catal. Letters. 64 (2000) 135–140, https://doi.org/10.1023/a:1019003523926.

[21] M.L. Hernández-Pichardo, P. Del Angel, J.A. Montoya-de la Fuente, Influence of the incorporation of Fe and Mn on the nanostructure and reactivity of catalysts based on tungstated zirconia, Catal. Today. 360 (2021) 72–77, https://doi.org/10.1016/j.cattod.2019.09.008.

[22] F.C. Jentoft, A. Hahn, J. Kröhnert, G. Lorenz, R.E. Jentoft, T. Ressler, U. Wild, R. Schlögl, C. Häßner, K. Köhler, Incorporation of manganese and iron into the zirconia lattice in promoted sulfated zirconia catalysts, J. Catal. 224 (1) (2004) 124–137, https://doi.org/10.1016/j.jcat.2004.02.012.

[23] D. Kaucký, Z. Sobalík, J.M. Hidalgo, R. Černý, O. Bortnovský, Impact of dopant metal ions in the framework of parent zirconia on the n-heptane isomerization activity of the Pt/WO3-ZrO2 catalysts, J. Mol. Catal. A Chem. 420 (2016) 107–114, https://doi.org/10.1016/j.molcata.2016.04.015.

[24] M.L. Hernandez-Pichardo, J.A.M.d.l. Fuente, P.D. Angel, A. Vargas, I. Hernández, M. González-Brambila, Optimization of manganese content by high-throughput experimentation of Pt/WO –ZrO2–Mn catalysts, Catal. Commun. 11 (5) (2010) 408–413, https://doi.org/10.1016/j.catcom.2009.11.010.

[25] D. Kaucký, B. Wichterlová, J. Dedecek, Z. Sobalik, I. Jakubec, Effect of the particle size and surface area of tungstated zirconia on the WOx nuclearity and n-heptane isomerization over Pt/WO 3-ZrO2, Appl. Catal. A Gen. 397 (1-2) (2011) 82–93, https://doi.org/10.1016/j.apcata.2011.02.020.

[26] J.P. Perdew, K. Burke, M. Ernzerhof, Generalized Gradient Approximation Made Simple, Phys. Rev. Lett. 77 (18) (1996) 3865–3868, https://doi.org/10.1103/PhysRevLett.77.3865.

[27] G. Kresse, D. Joubert, From ultrasoft pseudopotentials to the projector augmented-wave method, Phys. Rev. B. 59 (3) (1999) 1758–1775, https://doi.org/10.1103/PhysRevB.59.1758.

[28] P.E. Blöchl, Projector augmented-wave method, Phys. Rev. B. 50 (24) (1994) 17953–17979, https://doi.org/10.1103/PhysRevB.50.17953.

[29] G. Kresse, J. Furthmüller, Efficiency of ab-initio total energy calculations for metals and semiconductors using a plane-wave basis set, Comput. Mater. Sci. 6 (1) (1996) 15–50, https://doi.org/10.1016/0927-0256(96)00008-0.

[30] G. Kresse, J. Furthmüller, Efficient iterative schemes for ab initio total-energy calculations using a plane-wave basis set, Phys. Rev. B. 54 (16) (1996) 11169–11186, https://doi.org/10.1103/PhysRevB.54.11169.

[31] G. Kresse, J. Hafner, Ab initio molecular dynamics for liquid metals, Phys. Rev. B. 47 (1) (1993) 558–561, https://doi.org/10.1103/PhysRevB.47.558.

[32] G. Kresse, J. Hafner, Ab initio molecular-dynamics simulation of the liquid-metal–amorphous-semiconductor transition in germanium, Phys. Rev. B. 49 (20) (1994) 14251–14269, https://doi.org/10.1103/PhysRevB.49.14251.

[33] S. Grimme, J. Antony, S. Ehrlich, H. Krieg, A consistent and accurate ab initio parametrization of density functional dispersion correction (DFT-D) for the 94 elements H-Pu, J. Chem. Phys. 132 (15) (2010) 154104, https://doi.org/10.1063/1.3382344.

[34] S.L. Dudarev, G.A. Botton, S.Y. Savrasov, C.J. Humphreys, A.P. Sutton, Electron-energy-loss spectra and the structural stability of nickel oxide: An LSDA+U study, Phys. Rev. B. 57 (1998) 1505–1509, https://doi.org/10.1103/PhysRevB.57.1505.

[35] N.E. Kirchner-Hall, W. Zhao, Y. Xiong, I. Timrov, I. Dabo, Extensive Benchmarking of DFT+U Calculations for Predicting Band Gaps, Appl. Sci. 11 (2021) 2395, https://doi.org/10.3390/app11052395.

[36] H. Shin, A. Benali, Y.e. Luo, E. Crabb, A. Lopez-Bezanilla, L.E. Ratcliff, A. M. Jokisaari, O. Heinonen, Zirconia and hafnia polymorphs – ground state structural properties from diffusion Monte Carlo, Phys. Rev. Mater. 2 (7) (2018), https://doi.org/10.1103/PhysRevMaterials.2.075001.

[37] H.-Y. Chen, S. Tosoni, G. Pacchioni, Hydrogen Adsorption, Dissociation, and Spillover on Ru 10 Clusters Supported on Anatase TiO 2 and Tetragonal ZrO 2 (101) Surfaces, ACS Catal. 5 (9) (2015) 5486–5495, https://doi.org/10.1021/acscatal.5b01093.

[38] R.F.W. Bader, A quantum theory of molecular structure and its applications, Chem. Rev. 91 (5) (1991) 893–928, https://doi.org/10.1021/cr00005a013.

[39] C. Freysoldt, J. Neugebauer, C.G. Van de Walle, Fully Ab Initio Finite-Size Corrections for Charged-Defect Supercell Calculations, Phys. Rev. Lett. 102 (2009), 016402, https://doi.org/10.1103/PhysRevLett.102.016402.

[40] F. Bruneval, J.-P. Crocombette, X. Gonze, B. Dorado, M. Torrent, F. Jollet, Consistent treatment of charged systems within periodic boundary conditions: The projector augmented-wave and pseudopotential methods revisited, Phys. Rev. B. 89 (2014), 045116, https://doi.org/10.1103/PhysRevB.89.045116.

[41] A.J. Jones, E. Iglesia, The Strength of Brønsted Acid Sites in Microporous Aluminosilicates, ACS Catal. 5 (10) (2015) 5741–5755, https://doi.org/10.1021/acscatal.5b01133.